Significant Enhancement of Open-Circuit Voltage in Indoline-Based Dye-Sensitized Solar Cells via Retarding Charge Recombination

ARTICLE *in* CHEMISTRY OF MATERIALS · APRIL 2013

Impact Factor: 8.35 · DOI: 10.1021/cm400196w

7 AUTHORS, INCLUDING:

Zhihui Wang
Huaiyin Institute of Technology
11 PUBLICATIONS **152** CITATIONS
SEE PROFILE

Song Xue
Beijing Institute of Technology
110 PUBLICATIONS **1,003** CITATIONS
SEE PROFILE

ACS APPLIED MATERIALS & INTERFACES

Research Article

www.acsami.org

Judicious Design of Indoline Chromophores for High-Efficiency Iodine-Free Dye-Sensitized Solar Cells

Zhihui Wang,[†] He Wang,[†] Mao Liang,*[,†] Yulin Tan,[†] Fangyi Cheng,[‡] Zhe Sun,[†] and Song Xue*[,†]

[†]Tianjin Key Laboratory of Organic Solar Cells and Photochemical Conversion, Department of Applied Chemistry, Tianjin University of Technology, Tianjin 300384, People's Republic of China

[‡]Key Laboratory of Advanced Energy Materials Chemistry (KLAEMC) (Ministry of Education), Chemistry College, Nankai University, Tianjin 300071, People's Republic of China

Supporting Information

ABSTRACT: Indoline photosensitizers exhibit impressive short-circuit photocurrent but generally low molar extinction coefficient and rapid charge recombination, which limits their application in thin-film dye-sensitizerd solar cells (DSCs). Here, we incorporate a new dithieno[3,2-*b*:2′,3′-*d*]pyrrole (DTP) segment (i.e., dihexyloxy-triphenylamine (DHO-TPA) substituted DTP) as the conjugated π-linker to construct a series of high molar absorption coefficient indoline dyes (XW69, XW70, and XW71) for DSCs employing a cobalt(II/III) redox electrolyte. Interestingly, this DTP linker is demonstrated as an efficient building block, not only slowing down the kinetics of charge recombination of titania electrons with tris(1,10-phenanthroline)cobalt(III) ions but also making a great contribution to the light absorption properties in comparison with the dihexylaniline substituted DTP. With respect to the dihexyloxy-triphenylamine dye (XW68), these new indoline dyes exhibit stronger light-harvesting and thus better power conversion efficiency of DSCs made from thin titania films. Benefitting from the bulky rigidity of the donor and π-conjugation unit, the XW70 dye displays a promising conversion efficiency as high as 8.78%, with a short-circuit current density (J_{SC}) of 13.3 mA cm^{-2}, open-circuit voltage (V_{OC}) of 943 mV, and fill factor (FF) of 0.70 under AM 1.5 illumination (100 mW cm^{-2}). Furthermore, the effect of light irradiation on these dyes adsorbed on nanocrystalline TiO_2 films was investigated, proving the photostability of these indoline chromophores. Our work has valued the feasibility of judicious design of indoline chromophores to obtain organic photosensitizers for high-efficiency iodine-free DSCs made from thin titania films.

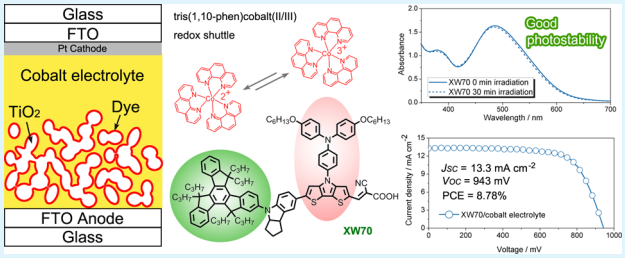

KEYWORDS: *indoline dyes, dithienopyrrole, truxene, photostability, dye-sensitized solar cell*

INTRODUCTION

Dye-sensitized solar cells (DSCs), as a new type of photovoltaic technology, have been considered to be a credible alternative to conventional inorganic silicon based solar cells because of their ease of fabrication, high efficiency, and cost effectiveness.[1] To achieve high solar power conversion efficiency, great research efforts are focused on designing and synthesizing new photosensitizers. The state-of-the-art DSC dyes are zinc porphyrin complexes, which have been demonstrated to convert solar light to electricity at a power efficiency of about 12%.[2] Meanwhile, metal-free organic dyes featuring intramolecular charge-transfer transitions have been attracting surging attention, because of their robust availability, ease of structural tuning, and generally high molar extinction coefficients.[3−23]

Indoline dye is one of the most powerful sensitizers, bearing the signs of good photoresponse in the visible region and high efficiency. Originally, Uchida and co-workers have reported a series of indoline dyes containing rhodanine-3-acetic acid (e.g., D205 and D149) as the acceptor and anchoring unit, showing high overall power conversion efficiencies (PCEs) of 8−9.5%.[24−28] Recently, Tian, Zhu, Wang, and co-workers developed a series of D−A−π−A indoline dyes with high power conversion efficiency as well as long-term stability.[4,6] An obvious advantage of the indoline dyes is their impressive photocurrent due to the powerful electron-donating capability of the indoline unit.[29] However, photovoltage is the key parameter hindering the further PCE improvement of indoline dye-sensitized DSCs.[30]

If the photovoltage of indoline dyes can be further improved, new breakthroughs would be expected for this type of dye. To deal with this topic, the judicious design of indoline dyes for iodine-free DSCs is one of the viable tactics. $Co^{II/III}$ polypyridyl redox couples have recently been proven quite successful as an alternative to the omnipresent triiodide/iodide redox shuttle in DSCs.[2,31−41] However, the significant control of charge recombination in these devices is a big challenge.[42] To the best of our knowledge, most of the indoline dye-correlated

Received: January 27, 2014
Accepted: March 25, 2014
Published: March 25, 2014

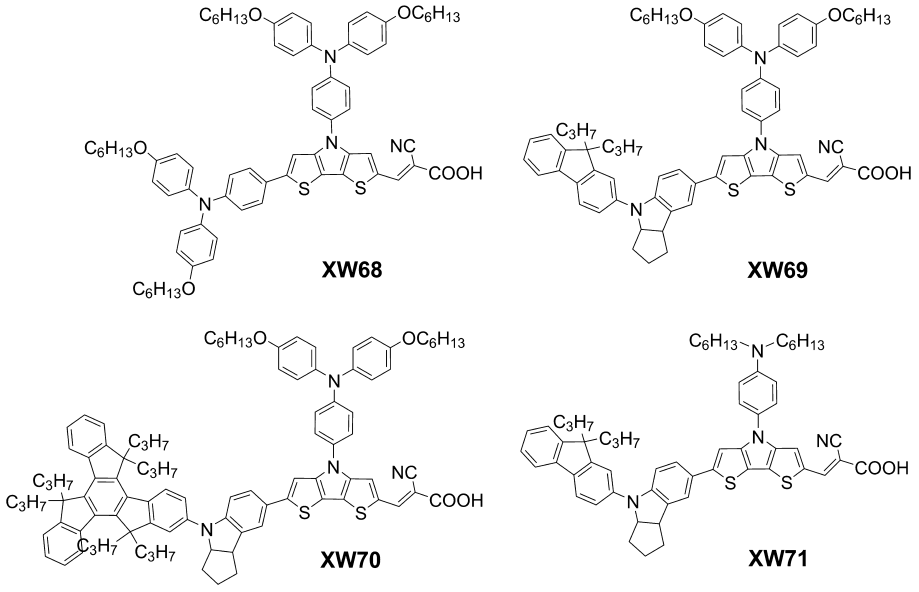

Figure 1. Molecular structures of dyes.

Scheme 1. Schematic Diagram for the Synthesized Dyes

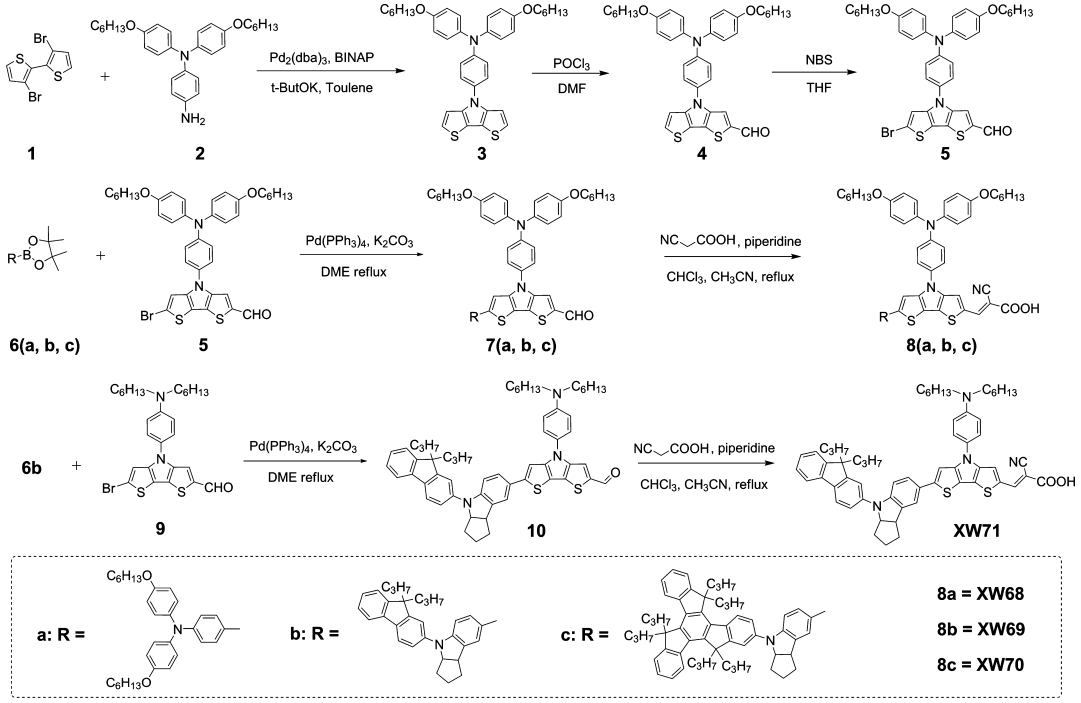

works were carried out only in the iodine electrolyte system, in which indoline dyes show generally low open-circuit voltage (below 800 mV).[3]

Thereby, in this contribution, we extended our work by employing two bulky dithieno[3,2-*b*:2′,3′-*d*]pyrrole (DTP) linkers, to construct three indoline dyes (XW69−XW71, Figure 1) featuring a higher absorption coefficient and a wider spectral response as compared to the reference dye, XW68 (Figure 1). The important finding to emerge from this study is that the feasibility of employing indoline organic dyes for high-efficiency DSCs employing the cobalt electrolyte has been demonstrated. In conjunction with a tris(1,10-phenanthroline)cobalt(II/III) redox couple, XW70 exhibits a PCE of 8.76% with an impressive photovoltage of 943 mV, the highest value obtained by indoline cells so far. We also scrutinize the effects of electron donor and linker structure in terms of light-harvesting, dynamic photoelectrochemical parameters,[43−48] as well as their joint contribution to the photovoltaic performance.

EXPERIMENTAL SECTION

Materials and Methods. The synthetic routes of XW68−XW71 are shown in Scheme 1. The starting materials of *N*′,*N*′-bis(4-(hexyloxy)phenyl)benzene-1,4-diamine **2** and boronic esters **6a**, **6b**, and **6c** were synthesized according to the reported literature.[39] 3,3′-Dibromo-2,2′-bithiophene, *n*-butyllithium, $Pd(PPh_3)_4$, $Pd_2(dba)_3$, $SnBu_3Cl$, *t*-BuONa, BINAP, and cyanoacetic acid were purchased from Energy Chemical (China). 4-*tert*-Butylpyridine (TBP) and 0.1 M lithium bis-(trifluoromethanesulfonyl)imide (LiTFSI) were purchased from Aldrich. *N*,*N*-Dimethylformamide was dried over and distilled

dx.doi.org/10.1021/am500575s | ACS Appl. Mater. Interfaces 2014, 6, 5768−5778

from CaH_2 under an atmosphere of nitrogen. Phosphorus oxychloride was freshly distilled before use. Dichloromethane (DCM) was distilled from calcium hydride under a nitrogen atmosphere. All other solvents and chemicals used in this work were analytical grade and used without further purification.

^1H NMR and ^{13}C NMR spectra were recorded on a Bruker AM-300 or AM-400 spectrometer. The reported chemical shifts were against TMS. High-resolution mass spectra were obtained with a Micromass GCT-TOF mass spectrometer. The melting point was taken on a RY-1 thermometer, and temperatures were uncorrected.

Optical and Electrochemical Measurements. The absorption spectra of dyes and sensitized films were measured by a SHIMADZU UV-2600 spectrophotometer. Fluorescence measurements were carried out with a HITACHI F-4500 fluorescence spectrophotometer.

Cyclic voltammetry (CV) measurements for sensitized films were performed on a Zennium electrochemical workstation (ZAHNER, Germany), with sensitized electrodes as the working electrode, Pt wires as the counter electrode, and a Ag/AgCl electrode as the reference electrode at a scan rate of 50 mV s^{-1}. Tetrabutylammonium perchlorate (TBAP, 0.1 M) and MeCN were used as supporting electrolyte and solvent, respectively. The results were calibrated using ferrocene as standard.

In this work, IMVS/EIS measurements were performed at completed dye-sensitized cells. Cell IMVS/EIS was measured in a two-electrode system with the cathode as a working electrode and the TiO_2-photoanode as the counter/reference electrodes. Charge densities at open circuit and intensity modulated photovoltage spectroscopy (IMVS) were performed on a Zennium electrochemical workstation (ZAHNER, Germany), which includes a green light-emitting diode (LED, 532 nm) and the corresponding control system. The intensity-modulated spectra were measured at room temperature with light intensity ranging from 5 to 75 W m^{-2}, in modulation frequency ranging from 0.1 Hz to 10 kHz, and with a modulation amplitude less than 5% of the light intensity. Electrochemical impedance spectroscopy (EIS) in the frequency range of 100 mHz to 100 kHz was performed with a Zennium electrochemical workstation (ZAHNER, Germany) in the dark with the alternate current amplitude set at 10 mV. Forward biases of 850 mV were applied to the dye-sensitized TiO_2 electrode during the measurement.

Theoretical Calculation Methods. The ground-state geometries were optimized in gas phase employing the hybrid B3LYP function9 and a 6-31+G basis set. Vertical excitation energies were calculated by time-dependent density functional theory (TD-DFT) at the B3LYP/6-31+G level of theory. All the calculations were carried out with Gaussian 09 program packages.[49] Note that the effect of the solvent (dichloromethane) on the absorption spectra has not been simulated. Optimized 3D structures were generated with the ChemBio3D ultra 11.0 program.

Fabrication and Characterization of DSCs. A 3.0 μm thick, single-layer titania film screen-printed on the FTO (Nippon Sheet Glass, Solar, 4 mm thick) conducting glass was used as the negative electrode. The TiO_2 electrode was stained by immersing it into a 0.3 mM dye solution in a mixture of dichloromethane (DCM)/EtOH (v/v, 1:4) and kept at room temperature for 36 h. The recipe of a Co-phen electrolyte: 0.25 M tris(1,10-phenanthroline)cobalt(II) di[bis-(trifluoromethanesulfonyl)imide], 0.05 M tris(1,10-phenanthroline)-cobalt(III) tris[bis(trifluoromethanesulfonyl)imide], 0.5 M TBP, and 0.1 M LiTFSI in MeCN. For comparison, an iodine electrolyte consisting of 0.25 M 1,2-dimethyl-3-*n*-propylimidazolium iodide (DMPImI), 0.1 M LiTFSI, 0.05 M I_2, and 0.5 M TBP in acetonitrile was formulated. Details on cell fabrication can be found in our previous publications.[50]

The photocurrent−voltage (J−V) characteristics of the solar cells were carried out using a Keithley 2400 digital source meter controlled by a computer and a standard AM 1.5 solar simulator, Oriel 91160-1000 (300W) SOLAR SIMULATOR 2 × 2 BEAM. The light intensity was calibrated by an Oriel reference solar cell. A metal mask with an aperture area of 0.2 cm^2 was covered on a testing cell during all measurements. The action spectra of monochromatic incident photon-to-current conversion efficiency (IPCE) for the solar cells were performed by using a commercial setup (QTest Station 2000 IPCE Measurement System, CROWNTECH, USA).

General Procedure for the Synthesis of Dyes XW68−XW71. To a stirred solution of compound **7a−7c** or **10** (0.2 mmol) and cyanoacetic acid (0.3 mmol) in acetonitrile (8 mL) was added chloroform (4 mL) and piperidine (0.6 mmol). The reaction mixture was refluxed for 8 h. Additional cyanoacetic acid (0.2 mmol) and piperidine (0.4 mmol) were added. The mixture was refluxed, which continued for 8 h, and then acidified with 1 M hydrochloric acid aqueous solution (30 mL). The crude product was extracted into CH_2Cl_2, washed with water, and dried over anhydrous $MgSO_4$. After removing solvent under reduced pressure, the residue was purified by column chromatography (DCM:CH_3OH = 10:1−3:1) to give the target dyes.

XW68. Red powder (93% yield). mp: 96−98 °C. IR (KBr): 3447, 2926, 1684, 1560, 1505, 1399, 1240, 827 cm^{-1}. ^1H NMR (400 MHz, $CDCl_3$): δ 8.27 (s, 1H), 7.75 (s, 1H), 7.41 (d, J = 8.0 Hz, 2H), 7.32 (d, J = 8.6 Hz, 2H), 7.16−7.14 (m, 5H), 7.07−7.05 (m, 6H), 6.91−6.88 (m, 6H), 6.85 (d, J = 8.6 Hz, 4H), 3.99−3.94 (m, 8H), 1.83−1.77 (m, 8H), 1.51−1.48 (m, 8H), 1.39−1.35 (m, 16H), 0.96−0.92 (m, 12H). ^{13}C NMR (100 MHz, $CDCl_3$): δ 156.0, 155.9, 150.8, 150.4, 149.3, 148.3, 144.4, 140.1, 139.9, 132.6, 130.9, 130.2, 128.8, 127.8, 127.1, 127.0, 126.5, 125.9, 124.1, 120.3, 119.6, 115.5, 115.4, 114.4, 105.8, 68.3, 31.6, 29.3, 25.8, 22.6, 14.0. HRMS (ESI) calcd for $C_{72}H_{81}N_4O_6S_2$ (M + H^+): 1161.5598, found: 1161.5623.

XW69. Red podwer (95% yield). mp: 104−106 °C. IR (KBr): 3445, 2927, 1673, 1603, 1568, 1504, 1398, 1241, 1157, 827 cm^{-1}. ^1H NMR (400 MHz, DMSO-d_6): δ 8.47 (s, 1H), 8.09 (s, 1H), 7.75 (d, J = 8.4 Hz, 1H), 7.70 (d, J = 7.6 Hz, 1H), 7.59 (s, 1H), 7.50−7.45 (m, 4H), 7.41−7.39 (m, 1H), 7.34 (s, 1H), 7.31−7.23 (m, 3H), 7.10 (d, J = 8.0 Hz, 4H), 6.95−6.93 (m, 5H), 6.89 (d, J = 8.0 Hz, 2H), 5.02−4.98 (m, 1H), 3.93 (t, J = 6.2 Hz, 4H), 3.87−3.83 (m, 1H), 2.08−2.04 (m, 1H), 1.97−1.93 (m, 4H), 1.88−1.81 (m, 2H), 1.79−1.75 (m, 1H), 1.73−1.63 (m, 6H), 1.43−1.38 (m, 4H), 1.33−1.27 (m, 8H), 0.87 (t, J = 6.0 Hz, 6H), 0.65−0.55 (m, 10H). ^{13}C NMR (100 MHz, $CDCl_3$): δ 156.0, 152.0, 150.8, 150.4, 148.1, 141.0, 140.2, 136.1, 135.5, 130.3, 127.1, 126.8, 126.2, 125.5, 124.1, 122.8, 120.4, 119.1, 119.0, 118.7, 117.2, 115.5, 114.4, 113.8, 107.7, 105.0, 68.3, 55.2, 42.9, 42.8, 31.6, 29.3, 25.8, 25.4, 22.6, 17.4, 17.3, 14.6, 14.5, 14.0. HRMS (ESI) calcd for $C_{72}H_{75}N_4O_4S_2$ (M + H^+): 1123.5230, found: 1123.5282.

XW70. Red powder (93% yield). mp: 204−206 °C. IR (KBr): 3446, 2926, 1601, 1505, 1399, 1242, 1157, 828, 749 cm^{-1}. ^1H NMR (400 MHz, DMSO-d_6): δ 8.51 (s, 1H), 8.31−8.28 (m, 3H), 8.13 (s, 1H), 7.66 (s, 1H), 7.60−7.52 (m, 6H), 7.47−7.38 (m, 6H), 7.14−7.12 (m, 5H), 6.95 (d, J = 8.4 Hz, 4H), 6.90 (d, J = 8.4 Hz, 2H), 5.08 (t, J = 6.4 Hz, 1H), 3.96−3.93 (m, 5H), 2.89−2.87 (m, 6H), 2.21−2.11 (m, 6H), 1.97−1.87 (m, 3H), 1.74−1.62 (m, 5H), 1.43−1.26 (m, 14H), 0.87 (t, J = 6.9 Hz, 6H), 0.56−0.45 (m, 30H). ^{13}C NMR (100 MHz, pyridine-d_5): δ 157.7, 157.1, 155.5, 155.4, 151.7, 150.6, 146.3, 145.8, 145.7, 145.0, 143.2, 142.1, 142.0, 141.9, 140.2, 140.1, 138.2, 137.2, 136.2, 135.7, 128.9, 128.6, 128.2, 127.2, 126.4, 125.6, 125.2, 124.2, 124.1, 122.3, 119.2, 117.4, 115.8, 114.4, 70.7, 69.8, 69.1, 57.6, 57.4, 57.3, 46.9, 41.0, 40.9, 36.5, 35.2, 33.0, 30.9, 27.3, 27.1, 26.0, 24.1, 19.3, 19.2, 16.1, 16.0, 15.9, 15.8, 15.4. HRMS (ESI) calcd for $C_{98}H_{107}N_4O_4S_2$ (M + H^+): 1467.7734, found: 1467.7759.

XW71. Red powder (90% yield). mp: 118−120 °C. IR (KBr): 3446, 3145, 2926, 1717, 1569, 1506, 1399, 1252, 1155, 741, 669 cm^{-1}. ^1H NMR (400 MHz, DMSO-d_6): δ 8.41 (s, 1H), 7.98 (s, 1H), 7.75 (d, J = 8.0 Hz, 1H), 7.70 (d, J = 7.6 Hz, 1H), 7.59 (s, 1H), 7.46−7.39 (m, 5H), 7.34 (s, 1H), 7.31−7.23 (m, 3H), 6.95 (s, J = 8.0 Hz, 1H), 6.78 (d, J = 8.0 Hz, 2H), 5.0 (t, J = 6.8 Hz, 1H), 3.86 (t, J = 6.8 Hz, 1H), 2.09−2.04 (m, 1H), 1.97−1.93 (m, 4H), 1.87−1.82 (m, 2H), 1.79−1.73 (m, 1H), 1.67−1.52 (m, 5H), 1.43−1.26 (m, 15H), 0.88 (t, J = 6.4 Hz, 6H), 0.65−0.54 (m, 12H). ^{13}C NMR (100 MHz, pyridine-d_5): δ 152.4, 150.6, 150.2, 149.1, 148.0, 147.7, 144.2, 142.0, 141.3, 136.5, 135.7, 134.7, 133.5, 127.2, 126.9, 126.6, 125.9, 125.7, 125.1, 123.7, 122.7, 122.5, 120.8, 119.3, 119.0, 114.5, 113.7, 112.6, 108.2, 106.1, 69.4, 55.4, 51.1, 45.3, 42.7, 42.6, 35.1, 33.5, 31.7, 27.4, 26.8, 24.4, 22.7, 17.6, 17.5, 14.5, 14.4, 14.0. HRMS (ESI) calcd for $C_{60}H_{67}N_4O_2S_2$ (M + H^+): 939.4705, found: 939.4760.

RESULTS AND DISCUSSION

Photophysical Properties. The UV−vis absorption spectra of the dyes in dichloromethane are depicted in Figure 2. The optical and electrochemical data of the dyes are summarized in Table 1. The absorption bands at 300−400 nm can be ascribed to the $\pi-\pi^*$ transitions of the conjugated system, whereas the bands in the range of 450−650 nm mainly stem from the intramolecular charge-transfer transition (ICT) from the electron donor to the cyanoacetic acid acceptor. In contrast with the small difference in the maximum absorption wavelength (λ_{max}, 533−553 nm), the molar extinction coefficients for XW68, XW69, XW70, and XW71 change to some different extent, located at 53 700, 69 800, 73 500, and 61 300 M^{-1} cm^{-1}, respectively.

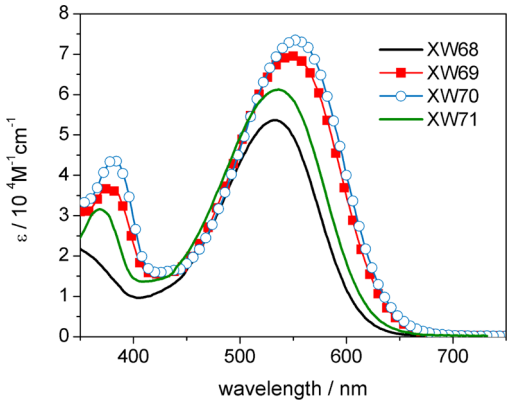

Figure 2. Absorption spectra of the dyes in dichloromethane.

Table 1. Electrochemical and Photophysical Properties of Dyes

dyes	λ_{max}/nm (ε/10^3 M^{-1} cm^{-1})[a]	E_{0-0}/V[b]	$E_{D/D+}$/V[c]	$E_{D^*/D+}$/V[d]
XW68	533 (53.7)	2.15	0.92	−1.23
XW69	378 (38.9), 544 (69.8)	2.06	0.89	−1.17
XW70	383 (43.6), 553 (73.5)	2.04	0.88	−1.16
XW71	378 (31.7), 536 (61.3)	2.09	0.84	−1.25

[a]The absorption spectra in DCM. [b]E_{0-0} values were estimated from the intersections of normalized absorption and emission spectra (λ_{int}, E_{0-0} = 1240/λ_{int}). [c]$E_{D/D+}$ was recorded by cyclic voltammograms of the dye-loaded TiO_2 film. [d]$E_{D^*/D+}$ was calculated from $E_{D/D+} - E_{0-0}$.

The bathochromic shift by 11 or 20 nm was observed when replacing the dihexyloxy substituted triphenylamine (DHO-TPA, XW68) unit with dipropylfluorene- or hexapropyltruxene substituted indoline (DPF-ID (XW69) or HPT-ID (XW70)) unit in the donor moiety, indicative of the more powerful electron-donating capability of the substituted indoline units than that of DHO-TPA. Note that there are hardly any electron donors that show stronger electron-donating ability than DHO-TPA. On the other hand, along with the distinct increase in molar extinction coefficient, the absorption peak of XW69 exhibits a 8 nm red-shift in absorption peak compared to that of XW71, indicating that the electron density of DHO-TPA substituted DTP is higher than that of dihexylaniline substituted DTP.

To gain insight into this conjugated linker correlated electron absorption spectra, we further performed quantum chemistry calculation with DFT and TDDFT methods (see Table 2). The results have shown that the observed ICT absorption band for XW71 stems mainly from the charge-transfer transition from HOMO (highest occupied molecular orbital) to LUMO (lowest occupied molecular orbital) (81.9%, f = 1.23), while a HOMO-to-LUMO transition combined with the transition from HOMO-1 to LUMO are observed for XW68−XW70. A phenomenon can be ascribed to the intrinsically photophysical feature of the DHO-TPA substituted DTP linker.

Table 2. Calculated Details of Electronic Transitions with the Relative Oscillator Strength Larger Than 0.5 of the Dyes

dyes	excited state	calculated energy (eV, nm)	oscillator strength (f)	transition assignment[a]
XW68	2	2.05, 604	0.89	H → L (23.3%)
				H-1 → L (62.3%)
XW69	2	2.12, 583	1.17	H → L (26.9%)
				H-1 → L (55.5%)
XW70	2	2.05, 604	1.06	H → L (65.6%)
				H-1 → L (20.2%)
XW71	1	2.14, 579	1.23	H → L (81.9%)
				H-2 → L (3.3%)

[a]H means HOMO, and L means LUMO.

Further insights into the electron distribution of the transition-involved frontier molecular orbitals are depicted in Figure 3. The observed LUMO for the XW68, XW69, XW70, and XW71 are similar, as expected. That is, the electron distribution of LUMO is delocalized through the DTP frame and cyanoacetic acid fragments with sizable contribution from the latter. However, the electron distribution of HOMO/HOMO-1 in XW68−XW70 is different from that of XW71. For example, the HOMO in XW69 is more delocalized than those in XW71. An apparent electron distribution on the DTP substituent (DHO-TPA unit) on HOMO/HOMO-1 orbitals can also be observed for XW68 and XW70. It is also worthy of noting that the exceptional electron-donor ability of a substituent on the DTP segment has hardly been reported. Recent studies on DTP moieties have suggested that most substituents on the DTP segment could be considered as an insulating spacer to reduce the intermolecular exciton annihilation in the assembly of dye molecules grafted on the surface of titania. There is no electron distribution on the DTP substituent[51,52] or DTP substituent-correlated transition probability is very low (<4%).[40] It seems that the lowest-energy absorption band of DTP dyes could not be tuned by molecular engineering of a DTP substituent. Nevertheless, this work has demonstrated that the DTP linker is more than just being an insulating spacer to reduce the intermolecular exciton annihilation in the assembly of dye molecules grafted on the surface of titania. Actually, the DHO-TPA based DTP linker could also make a great contribution to the light absorption properties as well as the electrochemical properties (see the next section) of dyes.

We further carried out cyclic voltammograms to determine the accurate $E_{D/D+}$ values of these dye-sensitized films (Table 1), by averaging the anodic and cathodic peak potentials (Figure 4). The oxidation potentials ($E_{D/D+}$, taken as the HOMO levels of the dyes) of XW68, XW69, XW70, and XW71 were measured to be 0.92, 0.89, 0.88, and 0.84 V versus a normal hydrogen electrode (NHE), respectively. Interestingly, the incorporation of a DHO-TPA based DTP linker is found to shift the $E_{D/D+}$ of dyes (XW68−XW70) to a more positive

dx.doi.org/10.1021/am500575s | ACS Appl. Mater. Interfaces 2014, 6, 5768−5778

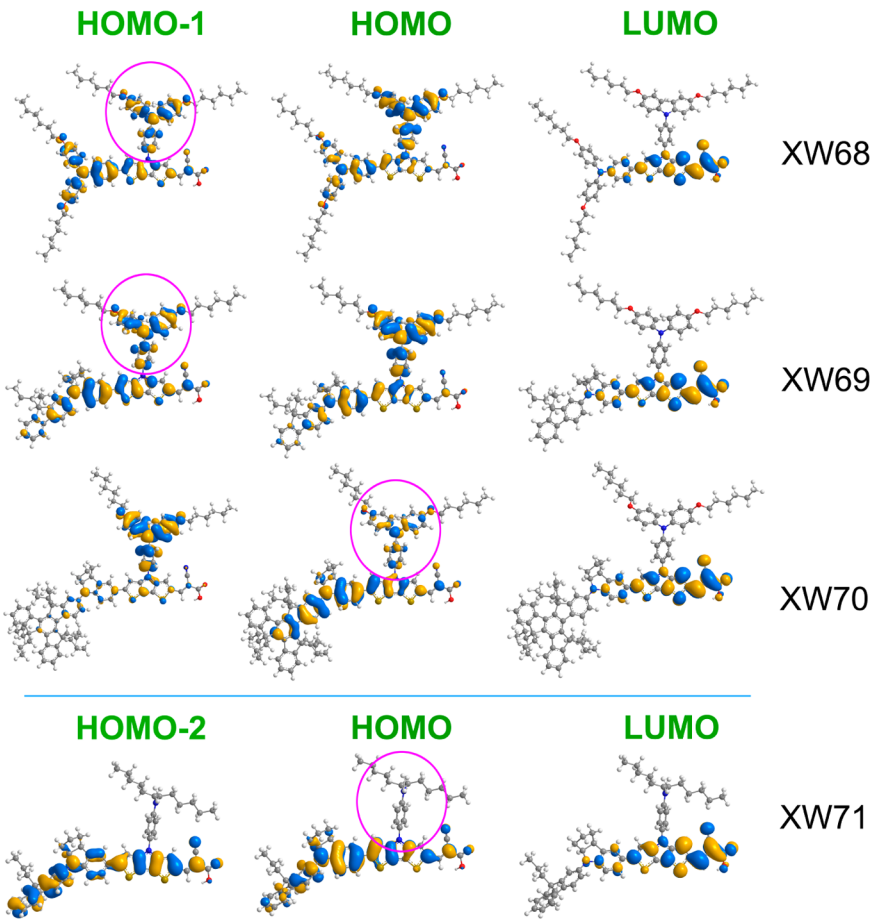

Figure 3. Frontier molecular orbitals of the dyes. The isodensity surface value was fixed at 0.2.

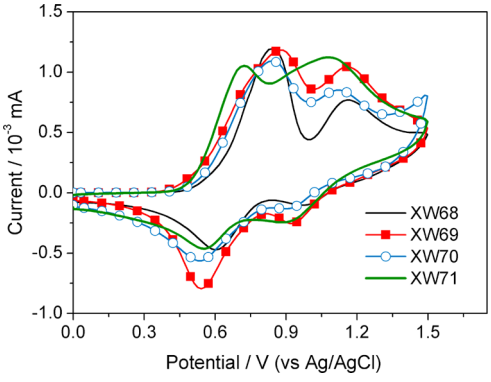

Figure 4. Cyclic voltammograms of the dye-loaded TiO_2 films.

potential, affording an increased Gibbs free energy for dye regeneration. In the present dyes (XW68−XW70), according to the frontier molecular isodensity plots Figure 3, the electron density is much more localized on the electron-rich DHO-TPA based DTP linker than on the terminal arylamine. Additionally, the HOMO/HOMO-1 is more delocalized in XW68−XW70 than the HOMO/HOMO-2 in XW71, which does not bear the same electron-rich substituent. Thus, the higher oxidation potential of XW68−XW70 compared to XW71 may come from this increased electronic delocalization on the linker substituent, resulting in a more difficult removal of the electron.

On the other hand, we could compute the $E_{D^*/D+}$ values of XW68−XW71 versus NHE via the equation $E_{D^*/D+} = E_{D/D+} - E_{0-0}$. According to the Franck−Condon principle, the zero−zero transition energies (E_{0-0}) were derived from the intersections of normalized absorption and emission spectra (Figure S1 in the Supporting Information). The principle states that, during an electronic transition, a change from one vibrational energy level to another will be more likely to happen if the two vibrational wave functions overlap more significantly. The LUMO of the XW68, XW69, XW70, and XW71 are calculated to be −1.23, −1.17, −1.16, and −1.25 V, respectively, indicative of thermodynamic feasibility for electron injection to conduction band (E_{CB}) of TiO_2 (−0.5 V versus NHE).

Photovoltaic Performance. The solar-to-electricity conversion efficiencies of DSCs made with XW68, XW69, XW70, and XW71 as the photosensitizers were examined by recording the photocurrent density−voltage (J−V) characteristics at the 100 mW cm^{-2}, simulated AM 1.5 conditions, and the detailed photovoltaic parameters are compiled in Table 3. As Figure 5 presents, the short-circuit photocurrent density (J_{SC}), open-circuit photovoltage (V_{OC}), and fill factor (FF) of the XW68 cell are 9.5 mA cm^{-2}, 900 mV, and 0.70, respectively, affording a power conversion efficiency (PCE) of 5.99%. Despite a slightly decreased V_{OC} of 861 mV, XW69 generates a remarkably improved J_{SC} of 12.2 mA cm^{-2}, contributing to a significantly enhanced PCE of 7.25%. This result confirms the promising potential of indoline dyes to achieve high performance for the thin film cobalt cells. Note that the DPF-ID/HPT-ID substituent has a profound influence on the photovoltaic behaviors of DSCs. For instance, the XW70 cell exhibits a notably improved V_{OC} of 943 mV concomitant with a slightly

dx.doi.org/10.1021/am500575s | ACS Appl. Mater. Interfaces 2014, 6, 5768−5778

Table 3. Photovoltaic Parameters for DSCs Employing the Cobalt or Iodine Electrolyte[a]

dye/electrolyte	J_{SC}/mA cm^{-2}	V_{OC}/mV	FF	PCE/%
XW68/cobalt	9.5	900	0.70	5.99
XW68/iodine	11.1	751	0.69	5.75
XW69/cobalt	12.2	861	0.69	7.25
XW69/iodine	13.1	732	0.70	6.71
XW70/cobalt	13.3	943	0.70	8.78
XW70/iodine	14.0	745	0.69	7.19
XW71/cobalt	12.7	845	0.69	7.40
XW71/iodine	13.8	720	0.68	6.76

[a]Irradiating light: AM 1.5G (100 mW cm^{-2}). The photovoltaic parameters are averaged values obtained from analysis of the $J-V$ curves of three identical working electrodes for each device fabricated and characterized under the same experimental conditions.

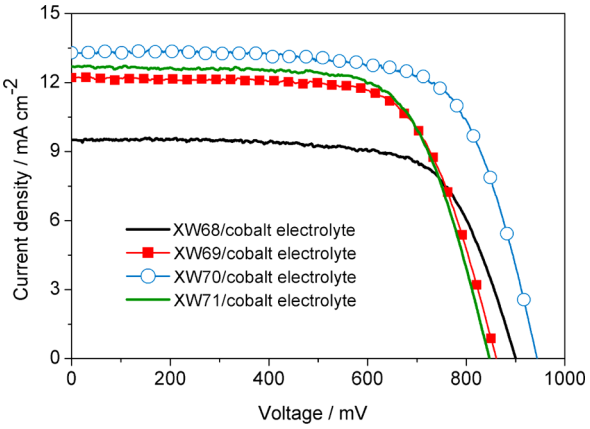

Figure 5. $J-V$ curves of the DSC devices studied employing the cobalt electrolyte under AM 1.5G simulated solar light (100 mW cm^{-2}).

increased J_{SC} of 13.3 mA cm^{-2} in comparison with the XW69 counterpart, resulting in a PCE improvement from 7.25% to 8.78%.

To verify the peculiar merit of the DPF-ID/HPT-ID organic dyes for DSCs made with thin TiO_2 films, we also performed $J-V$ characteristics of iodine cells based on the four dyes (photovoltaic data can be found in Table 3). An iodine control electrolyte consisting of 0.25 M 1,2-dimethyl-3-*n*-propylimidazolium iodide (DMPImI), 0.05 M iodine, 0.5 M TBP, and 0.1 M LiTFSI in acetonitrile was formulated to fabricate the iodine control cells. As Figure 6 presents, the XW69, XW70, and XW71 dyes display a better cell efficiency than XW68 (PCE = 5.75%). Upon employing the iodine electrolyte, the XW70 cell produced a J_{SC} of 14.0 mA cm^{-2}, V_{OC} of 745 mV, and FF of 0.69, corresponding to a PCE of 7.19%.

The incident photon-to-current conversion efficiency (IPCE) spectra for the cells were first examined in conjunction with a Co-phen electrolyte. As shown in Figure 7a, the XW70 dye exhibits a higher IPCE summit of 85% when compared to that of 79% for XW69, leading to a distinct increase in the J_{SC} value and thus the overall conversion efficiency. As we have known, IPCE is expressed by the product of light-harvesting efficiency (LHE) and absorbed photon-to-current conversion efficiency (APCE)[53]

$$\mathrm{IPCE}(\lambda) = \mathrm{LHE} \times \mathrm{APCE} = \mathrm{LHE} \times \eta_{col} \times \eta_{inj}$$

where APCE can be divided into two terms: the overall charge collective efficiency (η_{col}) and the overall electron injection

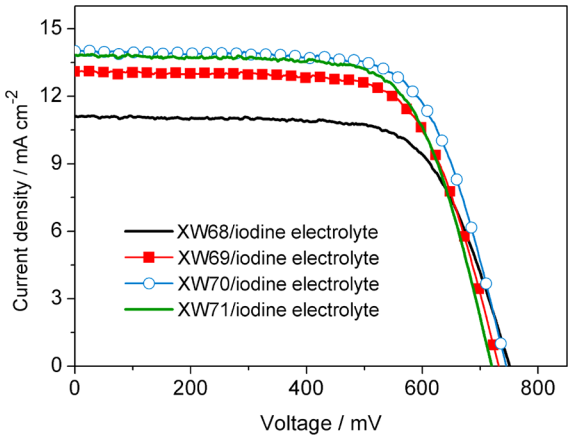

Figure 6. $J-V$ curves of the DSC devices studied employing the iodine electrolyte under AM 1.5G simulated solar light (100 mW cm^{-2}).

efficiency (η_{inj}). By looking at the electronic absorption spectra (Figure 7b) of 3 μm thick, dye-coated films, we can conclude that the light-harvesting efficiency is not the controlling factor for the IPCE difference of XW69 vs XW70. Note that XW68–XW71 sensitized films depict a fairly broad absorption plateau from 300 to 550 nm instead of distinguishable typical absorption bands in solution. On the other hand, the LUMOs of XW69 and XW70 are calculated to be −1.17 and −1.16 V, respectively, indicating that driving forces for electron injection are very similar for the two dyes. Thus, any difference in the photocurrent among DSCs based on XW69/XW70 could be attributed to the η_{col} difference. This deduction is in accordance with the electron lifetime characteristics of DSCs, as shown in the following discussion.

With respect to XW69/XW70, the XW68 sensitized cobalt cell shows lower photon-to-current conversion efficiencies over the 400–700 nm wavelength range, yielding a decreased integrated current density (9.5 mA cm^{-2}, Table 3). The IPCE attenuation of XW68 is primarily attributed to its narrower electronic absorption spectra (Figure 7b). Obviously, the alternation of electron donor from DHO-TPA to DPF-ID/HPT-ID strongly affects the short-circuit photocurrent density. This observation could be rationalized in terms of an evidently electron-richer character of the indoline groups than the DHO-TPA counterpart.

We further performed transient photovoltage decay measurements to dissect the origins of the aforementioned fluctuation of V_{OC} for the cobalt cells. The electron lifetime (τ) at open circuit, measured by controlled intensity modulated photovoltage spectroscopy (IMVS), can be obtained by fitting either the real or the imaginary part of the IMVS response (eqs 1 and 2).[54,55]

$$\mathrm{re}(\Delta V_{oc}) = \frac{X_1}{1 + (\omega\tau_{oc}^{re})^2} \quad (1)$$

$$\mathrm{im}(\Delta V_{oc}) = -\frac{X_2\omega\tau_{oc}^{im}}{1 + (\omega\tau_{oc}^{im})^2} \quad (2)$$

where $\mathrm{im}(\Delta V_{OC})$ is the imaginary modulation of the photopotential (ΔV_{OC}); $\mathrm{re}(\Delta V_{OC})$ is the real modulation of the photopotential (ΔV_{OC}); X_1, X_2, τ_{oc}^{re}, and τ_{oc}^{im} are the fit parameters; and ω is the circular frequency of the light modulation.

dx.doi.org/10.1021/am500575s | ACS Appl. Mater. Interfaces 2014, 6, 5768–5778

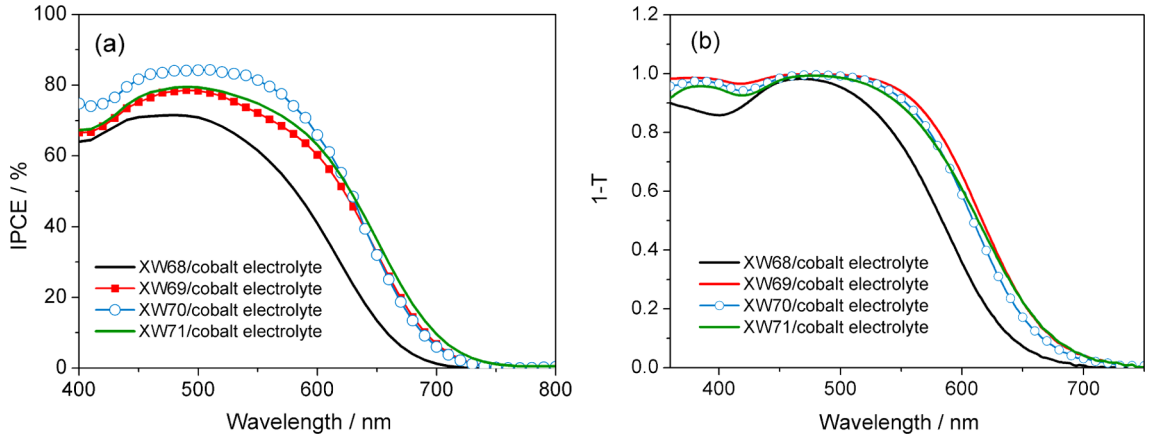

Figure 7. (a) IPCE action spectra of the studied DSCs employing cobalt electrolyte. (b) Absorption spectra of 3 μm thick, dye-coated titania films in contact with a Co-phen electrolyte for cell fabrication.

Figure 8 shows the electron lifetime as a function of extracted charge density (Q) at open circuit for the cobalt cells. The

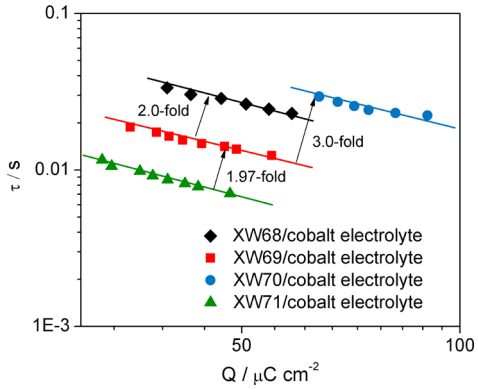

Figure 8. Electron lifetime as a function of electron density for the cobalt cells studied.

conjugated linker alteration from dihexylaniline substituted DTP (XW71) to DHO-TPA substituted DTP (XW69) has caused a 1.97-fold increased electron lifetime. This can be ascribed to the bulkier character of DHO-TPA substituted DTP, which, as pictorially illustrated in the upper panel of Figure 9a, keeps the cobalt(III) ions away from titania, slowing the interfacial charge recombination.

Furthermore, the dye alteration from XW69 to XW68 has caused a 2.0-fold increased electron lifetime. It is obvious that replacing the DPF-ID unit with DHO-TPA brings forth an evident deceleration of charge recombination. This can be ascribed to the bulkier three-dimensional character of the DHO-TPA electron donor in XW68. Interestingly, as depicted in Figure 8, it is easy to perceive that the XW70 cell presents a longer electron lifetime with respect to that of XW68. Note that the HPT-ID and DHO-TPA units have a similar profile of structure bulkiness (Figure 9b). The main difference between HPT-ID and DHO-TPA lies in the truxene unit, which makes the XW70 more rigid than XW69. The different character of the rigid truxene unit in XW70 in comparison with that of long alkyl chains in the DHO-TPA unit in XW68 can be well-understood by looking at the measured dye load amount: 2.42 $\times$ 10^{-8} mol cm^{-2} for XW68 and 1.26 $\times$ 10^{-8} mol cm^{-2} for XW70. The amount was obtained by comparing the absorbance change of a dye solution before and after dye uptaking with a

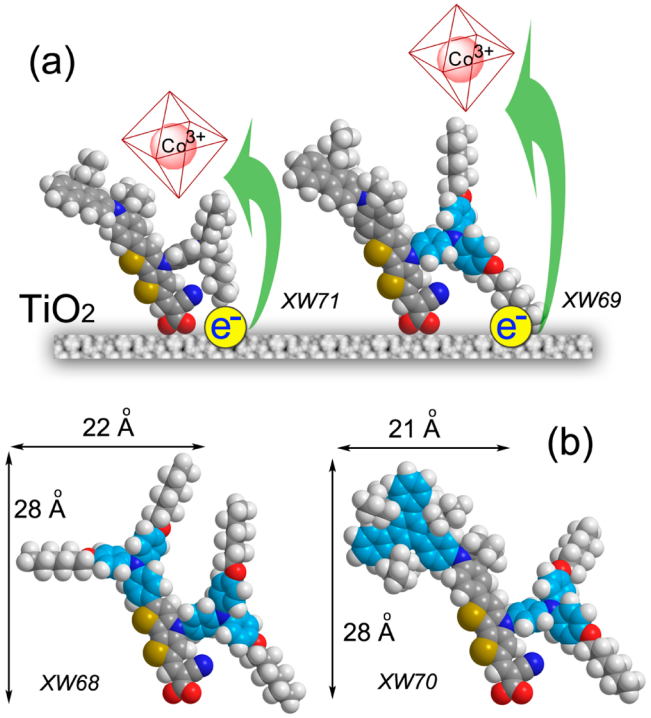

Figure 9. (a) Pictorial representation of the XW69 and XW71 on the titania surface. (b) The side view of the XW68 and XW70 derived from density functional theory (DFT) calculations (B3LYP).

titania film. The higher dye load amount of XW68 indicates that, under strong dye−dye intermolecular interaction between organic dyes owing to a large dipole moment, long alkyl chains could not keep their original spatial structure, as shown in Figure 9b. In contrast, this is not a problem in the case of XW70 containing the rigid truxene unit. This observation gives a distinct clue on the aforementioned electron lifetime dissimilarity. Furthermore, the superior ability of XW70 to control the interfacial charge recombination can be rationalized by measuring the electrochemical impedance spectroscopy (EIS) of devices. As shown in Figure 10, a major semicircle for each cobalt cell was observed in the Nyquist plot, which reflects the resistance of electron transport at the TiO_2/dye/electrolyte interface, i.e., the recombination kinetics between conduction-band electrons in TiO_2 and Co(III) ions from the electrolyte. The resistance values (R_{CT}) correspond to the diameters of the

dx.doi.org/10.1021/am500575s | ACS Appl. Mater. Interfaces 2014, 6, 5768−5778

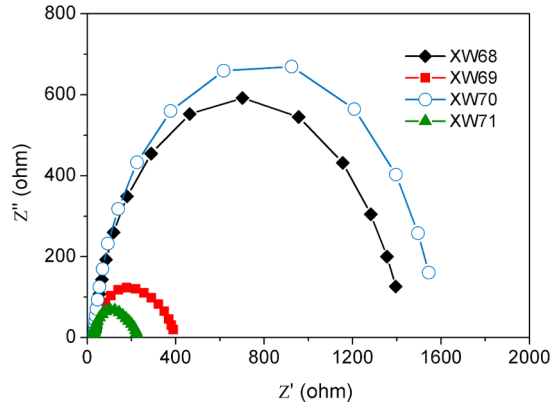

Figure 10. Nyquist plots of the cobalt cells studied.

semicircles; the larger the R_{CT}, the slower the recombination kinetics. Apparently, XW70 presents the largest R_{CT}, whereas XW71 generates the smallest one. This trend is in accordance with the electron lifetime characteristics of DSCs stated above.

Furthermore, the absorption spectra of the four dye-sensitized TiO_2 films before and after light irradiation were examined and are compared in Figure 11. A simple and efficient method was employed by Katoh,[56] Zhu,[6] and co-workers to evaluate the photostability of dyes in a short period of time. After 30 min of light irradiation on corresponding dye-sensitized TiO_2 electrodes, the absorbance of XW68, XW69, XW70, and XW71 maintained almost unchanged, indicating that no photochemical reaction occurred. This result has suggested that these D–π–A dyes featuring a DHO-TPA substituted DTP linker as well as the DPF-ID/HPT-ID moieties are stable enough under light irradiation as the precondition for a long-term stable device.

For further evaluating the practical stability of XW69 and XW70 based DSCs during a long term, a less volatile ionic liquid electrolyte consisting of 0.1 M LiI, 0.4 M I_2, and 0.4 M TBP in 1-methyl-3-*n*-propylimidazolium iodide (MPImI) was employed. Figure 12 shows the variations of photovoltaic parameters (J_{SC}, V_{OC}, FF, and PCE) with aging time for the

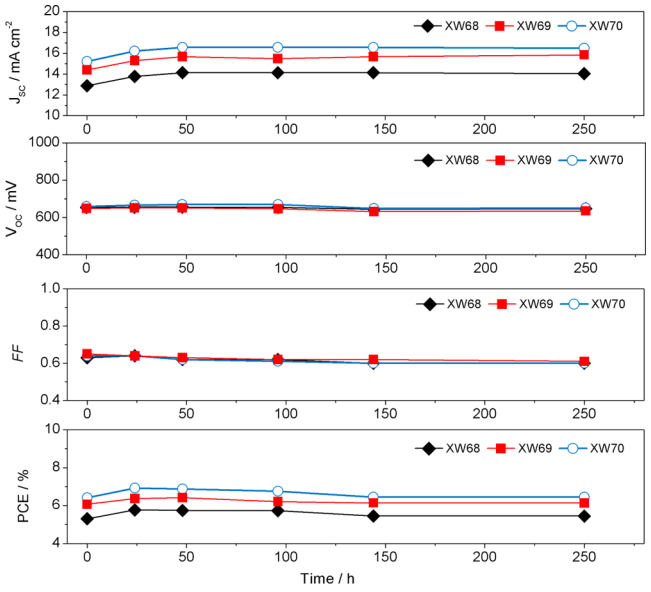

Figure 12. Variations of photovoltaic parameters (J_{SC}, V_{OC}, FF, and PCE) with aging time for the DSCs based on XW68, XW69, and XW70 under visible-light soaking.

DSCs based on XW68, XW69, and XW70 under visible-light soaking. The J_{SC} values obtained were 14.04, 15.84, and 16.47 mA cm^{-2} for XW68, XW69, and XW70, respectively, which are in the same order as those using liquid electrolyte. As expected, the J_{SC} values in the ionic liquid electrolyte cells are higher than those in the previously mentioned liquid electrolyte devices, owing to the increased film thickness (10 μm). Note that, for the dyes XW68, XW69, and XW70, small decreases in PCEs after 250 h of visible-light soaking were observed, indicating that the photostability of the indoline dyes is comparable to that of the DHO-TPA dyes. The resulting DSCs based on XW70 with ionic liquid electrolyte offered J_{SC} = 16.2 mA cm^{-2}, V_{OC} = 667 mV, and FF = 0.64, corresponding to a PCE of 6.91%.

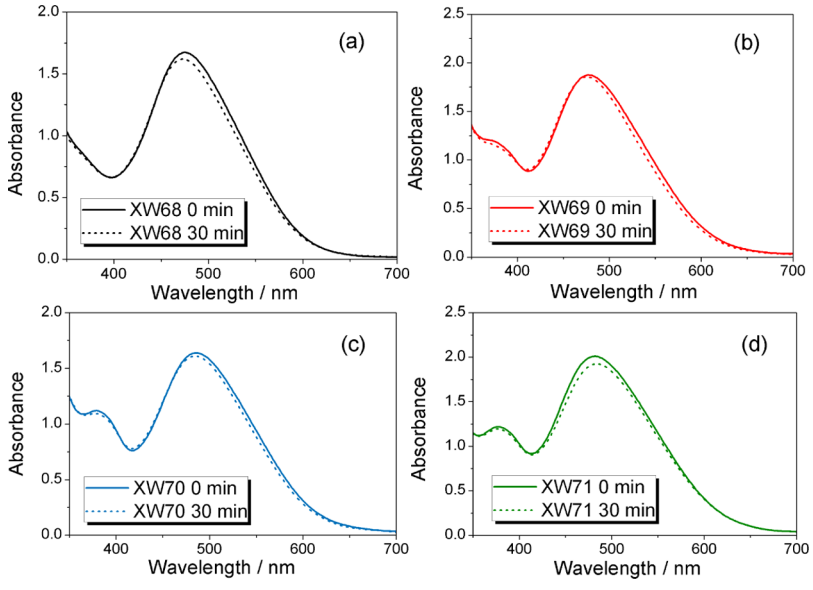

Figure 11. Absorption spectra of XW68 (a), XW69 (b), XW70 (c), and XW71 (d) sensitized TiO_2 films before and after light irradiation.

dx.doi.org/10.1021/am500575s | ACS Appl. Mater. Interfaces 2014, 6, 5768–5778

CONCLUSIONS

In summary, we have synthesized three new indoline dyes characteristic of a DHO-TPA substituted DTP linker, and the XW70 photosensitizer exhibits a good power conversion efficiency of 8.78% measured under the 100 mW cm^{-2}, simulated AM 1.5 sunlight, in combination with a noncorrosive Co-phen redox electrolyte. Theoretical calculations revealed that the DHO-TPA substituted DTP linker is more than just being an insulating spacer. This new linker displays quite a different electron distribution of transition-involved frontier molecular orbitals in comparison with other DTP linkers reported, making a great contribution to their light absorption properties. Furthermore, IMVS measurements have disclosed the critical influence of the indoline substituent upon the electron lifetime of cobalt cells, apart from the DTP linker, resulting in a considerably high V_{OC} of 943 mV in XW70 based DSCs. We further examined the effect of light irradiation on these dye-sensitized TiO_2 films, proving the photostability of these indoline chromophores. When applied in ionic liquid electrolyte DSCs, the indoline dyes, XW69 and XW70, also exhibit good photostability after 250 h of visible-light soaking. Our work should shed light on the future design of more powerful indoline photosensitizers for iodine-free dye-sensitized solar cells made from thin films.

ASSOCIATED CONTENT

Supporting Information

Synthesis and characterization of intermediates **3**−**5**, **7a**−**7c**, and **10** and normalized absorption and emission spectra of dyes in DCM. This material is available free of charge via the Internet at http://pubs.acs.org.

AUTHOR INFORMATION

Corresponding Authors

*Fax: +86 22 60214252. E-mail: liangmao717@126.com (M.L.).

*E-mail: xuesong@ustc.edu.cn (S.X.).

Notes

The authors declare no competing financial interest.

ACKNOWLEDGMENTS

We gratefully acknowledge the financial support from the National MOST (2011CBA00702), the National Natural Science Foundation of China (21373007, 21376179), and the Tianjin Natural Science Foundation (13JCZDJC32400).

REFERENCES

(1) O'Regan, B.; Grätzel, M. A Low-Cost, High-Efficiency Solar Cell Based on Dye-Sensitized Colloidal TiO_2 Films. *Nature* **1991**, *353*, 737−740.

(2) Yella, A.; Lee, H.; Tsao, H.; Yi, C.; Chandiran, A.; Nazeeruddin, M.; Diau, E.; Yeh, C.; Zakeeruddin, S.; Grätzel, M. Porphyrin-Sensitized Solar Cells with Cobalt (II/III)-Based Redox Electrolyte Exceed 12% Efficiency. *Science* **2011**, *334*, 629−634.

(3) Liang, M.; Chen, J. Arylamine Organic Dyes for Dye-Sensitized Solar Cells. *Chem. Soc. Rev.* **2013**, *42*, 3453−3488.

(4) Wu, Y. Z.; Zhu, W. H. Organic Sensitizers from D−π−A to D−A−π−A: Effect of the Internal Electron-Withdrawing Units on Molecular Absorption, Energy Levels and Photovoltaic Performances. *Chem. Soc. Rev.* **2013**, *42*, 2039−2058.

(5) Zhao, J.; Yang, X.; Cheng, M.; Li, S.; Sun, L. Molecular Design and Performance of Hydroxylpyridium Sensitizers for Dye-Sensitized Solar Cells. *ACS Appl. Mater. Interfaces* **2013**, *5*, 5227−5231.

(6) Pei, K.; Wu, Y.; Islam, A.; Zhang, Q.; Han, L.; Tian, H.; Zhu, W. Constructing High-Efficiency D−A−π−A-Featured Solar Cell Sensitizers: A Promising Building Block of 2,3-Diphenylquinoxaline for Antiaggregation and Photostability. *ACS Appl. Mater. Interfaces* **2013**, *5*, 4986−4995.

(7) Koh, T.; Nonomura, K.; Mathews, N.; Hagfeldt, A.; Grätzel, M.; G. Mhaisalkar, S.; C. Grimsdale, A. Influence of 4-*tert*-Butylpyridine in DSCs with $Co^{II/III}$ Redox Mediator. *J. Phys. Chem. C* **2013**, *117*, 15515−15522.

(8) Tingare, Y. S.; Shen, M.-T.; Su, C.; Ho, S.-Y.; Tsai, S.-H.; Chen, B.-R.; Li, W.-R. Novel Oxindole Based Sensitizers: Synthesis and Application in Dye-Sensitized Solar Cells. *Org. Lett.* **2013**, *15*, 4292−4295.

(9) Hart, A. S.; Bikram, K. C. C.; Subbaiyan, N. K.; Karr, P. A.; D'Souza, F. Phenothiazine-Sensitized Organic Solar Cells: Effect of Dye Anchor Group Positioning on the Cell Performance. *ACS Appl. Mater. Interfaces* **2012**, *4*, 5813−5820.

(10) Gou, F.; Jiang, X.; Li, B.; Jing, H.; Zhu, Z. Salicylic Acid As a Tridentate Anchoring Group for *azo*-Bridged Zinc Porphyrin in Dye-Sensitized Solar Cells. *ACS Appl. Mater. Interfaces* **2013**, *5*, 12631−12637.

(11) Ji, Z.; Natu, G.; Wu, Y. Cyclometalated Ruthenium Sensitizers Bearing a Triphenylamino Group for p-Type NiO Dye-Sensitized Solar Cells. *ACS Appl. Mater. Interfaces* **2013**, *5*, 8641−8648.

(12) Ning, Z.; Zhang, Q.; Pei, H.; Luan, J.; Lu, C.; Cui, Y.; Tian, H. Photovoltage Improvement for Dye-Sensitized Solar Cells via Cone-Shaped Structural Design. *J. Phys. Chem. C* **2009**, *113*, 10307−10313.

(13) De Sousa, S.; Olivier, C.; Ducasse, L.; Le Bourdon, G.; Hirsch, L.; Toupance, T. Oligocarbazole-Based Chromophores for Efficient Thin-Film Dye-Sensitized Solar Cells. *ChemSusChem* **2013**, *6*, 993−996.

(14) Paek, S.; Choi, H.; Choi, H.; Lee, C. W.; Kang, M. S.; Song, K.; Nazeeruddin, M. K.; Ko, J. Molecular Engineering of Efficient Organic Sensitizers Incorporating a Binary π-Conjugated Linker Unit for Dye-Sensitized Solar Cells. *J. Phys. Chem. C* **2010**, *114*, 14646−14653.

(15) Liang, M.; Xu, W.; Cai, F. S.; Chen, P. Q.; Peng, B.; Chen, J.; Li, Z. M. New Triphenylamine-Based Organic Dyes for Efficient Dye-Sensitized Solar Cells. *J. Phys. Chem. C* **2007**, *111*, 4465−4472.

(16) Liang, Y.; Peng, B.; Liang, J.; Tao, Z.; Chen, J. Triphenylamine-Based Dyes Bearing Functionalized 3,4-Propylenedioxythiophene Linkers with Enhanced Performance for Dye-Sensitized Solar Cells. *Org. Lett.* **2010**, *12*, 1204−1207.

(17) Liang, Y.; Cheng, F.; Liang, J.; Chen, J. Triphenylamine-Based Ionic Dyes with Simple Structures: Broad Photoresponse and Limitations on Open-Circuit Voltage in Dye-Sensitized Solar Cells. *J. Phys. Chem. C* **2010**, *114*, 15842−15848.

(18) Ren, X.; Feng, Q.; Zhou, G.; Huang, C.-H.; Wang, Z.-S. Effect of Cations in Coadsorbate on Charge Recombination and Conduction Band Edge Movement in Dye-Sensitized Solar Cells. *J. Phys. Chem. C* **2010**, *114*, 7190−7195.

(19) Chen, C.; Liao, J.-Y.; Chi, Z.; Xu, B.; Zhang, X.; Kuang, D.-B.; Zhang, Y.; Liu, S.; Xu, J. Metal-Free Organic Dyes Derived from Triphenylethylene for Dye-Sensitized Solar Cells: Tuning of the Performance by Phenothiazine and Carbazole. *J. Mater. Chem.* **2012**, *22*, 8994−9005.

(20) Lu, M.; Liang, M.; Han, H.; Sun, Z.; Xue, S. Organic Dyes Incorporating Bis-hexapropyltruxeneamino Moiety for Efficient Dye-Sensitized Solar Cells. *J. Phys. Chem. C* **2011**, *115*, 274−281.

(21) Hao, X.; Liang, M.; Cheng, X.; Pian, X.; Sun, Z.; Xue, S. Organic Dyes Incorporating the Benzo[1,2-*b*:4,5-*b*′]dithiophene Moiety for Efficient Dye-Sensitized Solar Cells. *Org. Lett.* **2011**, *13*, 5424−5427.

(22) Zhang, Y.; Zhang, Y.; Wang, Z.; Liang, M.; Jia, D.; Wu, Q.; Xue, S. Effects of Different Alkyl Chains on the Performance of Dye-Sensitized Solar Cells with Different Electrolytes. *J. Power Sources* **2014**, *253*, 167−176.

(23) Hao, Y.; Liang, M.; Wang, Z.; Wang, L.; Sun, Y.; Sun, Z.; Xue, S. 3,4-Ethylenedioxythiophene as an Electron Donor to Construct Arylamine Sensitizers for Highly Efficient Iodine-Free Dye-Sensitized Solar Cells. *Phys. Chem. Chem. Phys.* **2013**, *15*, 15441−15449.

(24) Horiuchi, T.; Miura, H.; Uchida, S. Highly-Efficient Metal-Free Organic Dyes for Dye-Sensitized Solar Cells. *Chem. Commun.* **2003**, 3036−3037.
(25) Horiuchi, T.; Miura, H.; Sumioka, K.; Uchida, S. High Efficiency of Dye-Sensitized Solar Cells Based on Metal-Free Indoline Dyes. *J. Am. Chem. Soc.* **2004**, *126*, 12218−12219.
(26) Ito, S.; Zakeeruddin, S. M.; Humphry-Baker, R.; Liska, P.; Charvet, R.; Comte, P.; Nazeeruddin, M. K.; Péchy, P.; Takata, M.; Miura, H.; Uchida, S.; Grätzel, M. High-Efficiency Organic-Dye-Sensitized Solar Cells Controlled by Nanocrystalline-TiO_2 Electrode Thickness. *Adv. Mater.* **2006**, *18*, 1202−1205.
(27) Ito, S.; Miura, H.; Uchida, S.; Takata, M.; Sumioka, K.; Liska, P.; Comte, P.; Pechy, P.; Grätzel, M. High-Conversion-Efficiency Organic Dye-Sensitized Solar Cells with a Novel Indoline Dye. *Chem. Commun.* **2008**, 5194−5196.
(28) Kuang, D.; Uchida, S.; Humphry-Baker, R.; Zakeeruddin, S. M.; Grätzel, M. Organic Dye-Sensitized Ionic Liquid Based Solar Cells: Remarkable Enhancement in Performance through Molecular Design of Indoline Sensitizers. *Angew. Chem., Int. Ed.* **2008**, *47*, 1923−1927.
(29) Zhu, W. H.; Wu, Y.; Wang, S.; Li, W.; Li, X.; Chen, J.; Wang, Z. S.; Tian, H. Organic D-A-π-A Solar Cell Sensitizers with Improved Stability and Spectral Response. *Adv. Funct. Mater.* **2011**, *21*, 756−763.
(30) Li, G.; Liang, M.; Wang, H.; Sun, Z.; Wang, L.; Wang, Z. H.; Xue, S. Significant Enhancement of Open-Circuit Voltage in Indoline-Based Dye-Sensitized Solar Cells via Retarding Charge Recombination. *Chem. Mater.* **2013**, *25*, 1713−1722.
(31) Zhang, M.; Wang, Y.; Xu, M.; Ma, W.; Li, R.; Wang, P. Design of High-Efficiency Organic Dyes for Titania Solar Cells Based on the Chromophoric Core of Cyclopentadithiophene-benzothiadiazole. *Energy Environ. Sci.* **2013**, *6*, 2944−2949.
(32) Bai, Y.; Zhang, J.; Zhou, D.; Wang, Y.; Zhang, M.; Wang, P. Engineering Organic Sensitizers for Iodine-Free Dye-Sensitized Solar Cells: Red-Shifted Current Response Concomitant with Attenuated Charge Recombination. *J. Am. Chem. Soc.* **2011**, *133*, 11442−11445.
(33) Xu, M.; Zhang, M.; Pastore, M.; Li, R.; De Angelis, F.; Wang, P. Joint Electrical, Photophysical and Computational Studies on D-π-A Dye Sensitized Solar Cells: The Impacts of Dithiophene Rigidification. *Chem. Sci.* **2012**, *3*, 976−983.
(34) Feldt, S. M.; Gibson, E. A.; Gabrielsson, E.; Sun, L.; Boschloo, G.; Hagfeldt, A. Design of Organic Dyes and Cobalt Polypyridine Redox Mediators for High-Efficiency Dye-Sensitized Solar Cells. *J. Am. Chem. Soc.* **2010**, *132*, 16714−16724.
(35) Yum, J.-H.; Baranoff, E.; Kessler, F.; Mmoehl, T.; Ahmad, S.; Bessho, T.; Mmarchioro, A.; Ghadiri, E.; Mmoser, J.-E.; Yi, C.; Nnazeeruddin, M. K.; Grätzel, M. A Cobalt Complex Redox Shuttle for Dye-Sensitized Solar Cells with High Open-Circuit Potentials. *Nat. Commun.* **2012**, *3*, 631.
(36) Kashif, M. K.; Axelson, J. C.; Duffy, N. W.; Forsyth, C. M.; Chang, C. J.; Long, J. R.; Spiccia, L.; Bach, U. A New Direction in Dye-Sensitized Solar Cells Redox Mediator Development: In Situ Fine-Tuning of the Cobalt(II)/(III) Redox Potential through Lewis Base Interactions. *J. Am. Chem. Soc.* **2012**, *134*, 16646−16653.
(37) Zong, X. P.; Liang, M.; Fan, C. R.; Tang, K.; Li, G.; Sun, Z.; Xue, S. Design of Truxene-Based Organic Dyes for High-Efficiency Dye-Sensitized Solar Cells Employing Cobalt Redox Shuttle. *J. Phys. Chem. C* **2012**, *116*, 11241−11250.
(38) Zong, X. P.; Liang, M.; Chen, T.; Jia, J. N.; Wang, L. N.; Sun, Z.; Xue, S. Efficient Iodine-Free Dye-Sensitized Solar Cells Employing Truxene-Based Organic Dyes. *Chem. Commun.* **2012**, *48*, 6645−6647.
(39) Wang, Z. H.; Liang, M.; Wang, L.; Hao, Y.; Wang, C.; Sun, Z.; Xue, S. New Triphenylamine Organic Dyes Containing Dithieno[3,2-*b*:2′,3′-*d*]pyrrole (DTP) Units for Iodine-Free Dye-Sensitized Solar Cells. *Chem. Commun.* **2013**, *49*, 5748−5750.
(40) Wang, Z. H.; Liang, M.; Hao, Y.; Zhang, Y.; Wang, L.; Sun, Z.; Xue, S. Influence of the N-Heterocycle Substituent of the Dithieno-[3,2-*b*:2′,3′-*d*]pyrrole (DTP) Spacer as Well as Sensitizer Adsorption Time on the Photovoltaic Properties of Arylamine Organic Dyes. *J. Mater. Chem. A* **2013**, *1*, 11809−11819.
(41) Wang, Z. H.; Liang, M.; Wang, H.; Wang, P.; Cheng, F.; Sun, Z.; Xue, S. Joint Electrical, Photophysical, and Photovoltaic Studies on Truxene Dye-Sensitized Solar Cells: Impact of Arylamine Electron Donors. *ChemSusChem* **2014**, *7*, 795−803.
(42) Wang, H.; Sun, Z.; Zhang, Y. K.; Zhang, Y.; Liang, M.; Jia, D. D.; Xue, S. Charge Transport Limitations of Redox Mediators in Dye-Sensitized Solar Cells: Investigation Based on a Quasi-Linear Model. *J. Phys. Chem. C* **2014**, *118*, 60−70.
(43) Wang, H.; Peter, L. M. Influence of Electrolyte Cations on Electron Transport and Electron Transfer in Dye-Sensitized Solar Cells. *J. Phys. Chem. C* **2012**, *116*, 10468−10475.
(44) Das, S. K.; Song, B.; Mahler, A.; Nesterov, V. N.; Wilson, A. K.; Ito, O.; D'Souza, F. Electron Transfer Studies of High Potential Zinc Porphyrin−Fullerene Supramolecular Dyads. *J. Phys. Chem. C* **2014**, *118*, 3994−4006.
(45) Liu, Y.; Jennings, J. R.; Huang, Y.; Wang, Q.; Zakeeruddin, S. M.; Grätzel, M. Cobalt Redox Mediators for Ruthenium-Based Dye-Sensitized Solar Cells: A Combined Impedance Spectroscopy and Near-IR Transmittance Study. *J. Phys. Chem. C* **2011**, *115*, 18847−18855.
(46) Brennan, T. P.; Tanskanen, J. T.; Bakke, J. R.; Nguyen, W. H.; Nordlund, D.; Toney, M. F.; McGehee, M. D.; Sellinger, A.; Bent, S. F. Molecular Engineering of Organic Dyes for Improved Recombination Lifetime in Solid-State Dye-Sensitized Solar Cells. *Chem. Mater.* **2013**, *25*, 4354−4363.
(47) Hoff, D. A.; Silva, R. d.; Rego, L. G. C. Coupled Electron−Hole Quantum Dynamics on D−π−A Dye-Sensitized TiO_2 Semiconductors. *J. Phys. Chem. C* **2012**, *116*, 21169−21178.
(48) Liu, Y.; Lin, H.; Dy, J. T.; Tamaki, K.; Nakazaki, J.; Nishiyama, C.; Uchida, S.; Segawa, H.; Li, J. Kinetics versus Energetics in Dye-Sensitized Solar Cells Based on an Ethynyl-Linked Porphyrin Heterodimer. *J. Phys. Chem. C* **2014**, *118*, 1426−1435.
(49) Frisch, M. J.; Trucks, G. W.; Schlegel, H. B.; Scuseria, G. E.; Robb, M. A.; Cheeseman, J. R.; Zakrzewski, V. G.; Montgomery, J. A.; Stratmann, R. E.; Burant, J. C.; Dapprich, S.; Millam, J. M.; Daniels, A. D.; Kudin, K. N.; Strain, M. C.; Farkas, O.; Tomasi, J.; Barone, V.; Cossi, M.; Cammi, R.; Mennucci, B.; Pomelli, C.; Adamo, C.; Clifford, S.; Ochterski, J.; Petersson, G. A.; Ayala, P. Y.; Cui, Q.; Morokuma, K.; Malick, D. K.; Rabuck, A. D.; Raghavachari, K.; Foresman, J. B.; Cioslowski, J.; Ortiz, J. V.; Stefanov, B. B.; Liu, G.; Liashenko, A.; Piskorz, P.; Komaromi, I.; Gomperts, R.; Martin, R. L.; Fox, D. J.; Keith, T.; Al-Laham, M. A.; Peng, C. Y.; Nanayakkara, A.; Gonzalez, C.; Challacombe, M.; Gill, P. M. W.; Johnson, B. G.; Chen, W.; Wong, M. W.; Andres, J. L.; Head-Gordon, M.; Replogle, E. S.; Pople, J. A. *Gaussian 09*; Gaussian, Inc.: Wallingford, CT, 2009.
(50) Shi, Y.; Liang, M.; Wang, L.; Han, H.; You, L.; Sun, Z.; Xue, S. New Ruthenium Sensitizers Featuring Bulky Ancillary Ligands Combined with a Dual Functioned Coadsorbent for High Efficiency Dye-Sensitized Solar Cells. *ACS Appl. Mater. Interfaces* **2013**, *5*, 144−153.
(51) Cai, N.; Zhang, J.; Xu, M.; Zhang, M.; Wang, P. Improving the Photovoltage of Dithienopyrrole Dye-Sensitized Solar Cells via Attaching the Bulky Bis(octyloxy)biphenyl Moiety to the Conjugated π-Linker. *Adv. Funct. Mater.* **2013**, *23*, 3539−3547.
(52) Zhang, J.; Yao, Z.; Cai, Y.; Yang, L.; Xu, M.; Li, R.; Zhang, M.; Dong, X.; Wang, P. Conjugated Linker Correlated Energetics and Kinetics in Dithienopyrrole Dye-Sensitized Solar Cells. *Energy Environ. Sci.* **2013**, *6*, 1604−1614.
(53) Wang, X.; Tamiaki, H.; Wang, L.; Tamai, N.; Kitao, O.; Zhou, H. S.; Sasaki, S. Chlorophyll-*a* Derivatives with Various Hydrocarbon Ester Groups for Efficient Dye-Sensitized Solar Cells: Static and Ultrafast Evaluations on Electron Injection and Charge Collection Processes. *Langmuir* **2010**, *26*, 6320−6327.
(54) Schlichthörl, G.; Huang, S. Y.; Sprague, J.; Frank, A. J. Band Edge Movement and Recombination Kinetics in Dye-Sensitized Nanocrystalline TiO_2 Solar Cells: A Study by Intensity Modulated Photovoltage Spectroscopy. *J. Phys. Chem. B* **1997**, *101*, 8141−8155.

(55) Schlichtho1rl, G.; Park, N. G.; Frank, A. J. Evaluation of the Charge-Collection Efficiency of Dye-Sensitized Nanocrystalline TiO_2 Solar Cells. *J. Phys. Chem. B* **1999**, *103*, 782−791.
(56) Katoh, R.; Furube, A.; Mori, S.; Miyashita, M.; Sunahara, K.; Koumura, N.; Hara, K. Highly Stable Sensitizer Dyes for Dye-Sensitized solar Cells: Role of the Oligothiophene Moiety. *Energy Environ. Sci.* **2009**, *2*, 542−546.